NASA CR-11220

FURTHER ANALYTICAL STUDY OF HYBRID ROCKET COMBUSTION

Final Report

NASI-10210, Task Order No. 3

Submitted to:

National Aeronautics and Space Administration
Langley Research Center
Hampton, Virginia 23365

Submitted by:

W.S.Y. Hung, C.S. Chen and J.K. Haviland

Report No. AEEP-4041-106-72U

October 1972

FURTHER ANALYTICAL STUDY OF HYBRID ROCKET COMBUSTION

Final Report

NASI-10210, Task Order No. 3

Submitted to:

National Aeronautics and Space Administration
Langley Research Center
Hampton, Virginia 23365

Submitted by:

W.S.Y. Hung, H.C. S. Chen and J.K. Haviland

Divisions of Mechanical and Aerospace Engineering
RESEARCH LABORATORIES FOR THE ENGINEERING SCIENCES
SCHOOL OF ENGINEERING AND APPLIED SCIENCE
UNIVERSITY OF VIRGINIA
CHARLOTTESVILLE, VIRGINIA

Report No. AEEP-4041-106-72U

Copy No.____

October 1972

ABSTRACT

This work utilized the computational techniques initially developed under NASA Grant No. NGR-47-005-085 and refined under NASA Contract No. NASI-10210, Task Order No.2, to carry out further analytical studies of the transient and steady-state combustion processes in a hybrid rocket system. The particular system chosen consists of a gaseous oxidizer flowing within a tube of solid fuel, resulting in a heterogeneous combustion. Finite rate chemical kinetics with appropriate reaction mechanisms were incorporated in the model. A temperature dependent Arrhenius type fuel surface regression rate equation was chosen for the current study. The governing mathematical equations employed for the reacting gas phase and for the solid phase are the general, two-dimensional, time-dependent conservation equations in a cylindrical coordinate system. Keeping the simplifying assumptions to a minimum, these basic equations were programmed for numerical computation, using two implicit finite-difference schemes, the Lax-Wendroff scheme for the gas phase, and, the Crank-Nicolson scheme for the solid phase. Appropriate initial and boundary conditions were represented, including heat and mass conservation at the gas-solid interface. A favorable downstream pressure gradient was imposed in order to obtain numerical solutions. In this study, Plexiglas (PMM) and oxygen (O_2) were selected as the fuel and the oxidizer, respectively. A single overall irreversible chemical reaction, such as fuel + oxidizer → product, was used for the gas-phase chemical reaction to economize computing time. Constant property models were employed, using equivalent turbulent values for the transport properties. The initial and boundary conditions were chosen to simulate the conditions at the start of the ignition process when a fully-developed flow of preheated oxygen reaches the inlet of the combustion chamber. Numerical calculations were performed for six cases with various values of flow rate and chamber pressure. Analyses were made primarily of the steady-state regression rate as a function of the axial position. The results were discussed. Conclusions have been drawn and recommendations have been made.

TABLE OF CONTENTS

LIST OF TABLES

LIST OF FIGURES

LIST OF SYMBOLS

$\hat{C}_p$	$\frac{C_p}{C_{po}}$
C_p	Specific heat per unit mass of gas mixture at constant pressure
$\hat{C}_s$	$\frac{C_s}{C_{so}}$
C_s	Specific heat per unit mass of solid fuel
Da	Damkohler number, $\frac{r_o W_o}{\rho_o V_o}$
$\hat{D}_i$	$\frac{D_i}{D_o}$
D_i	Binary diffusion coefficient of the i^{th} chemical species into the rest
Ec	Eckert number, $\frac{V_o^2}{C_{po} T_o}$
G_{xi_o}	Oxidizer mass flow rate per unit area at inlet
$\hat{h}$	$\frac{h}{C_{po} T_o}$
h	Enthalpy per unit mass of gas mixture
$\hat{h}_i^o$	$\frac{h_i^o}{C_{po} T_o}$
h_i^o	Heat of formation per unit mass of the i^{th} chemical species
$\hat{h}_{Li}$	$\frac{h_{Li}}{C_{po} T_o}$
h_{Li}	Latent heat per unit mass of the i^{th} chemical species due to phase change

LIST OF SYMBOLS (continued)

l	Molal volume of chemical species
k	Rate constant
LFL	Lower flammability limit
$\hat{P}$	$\frac{P}{\rho_o v_o^2}$
P	Static pressure of gas mixture
Pr	Prandtl number, $\frac{C_{po}\mu_o}{\lambda_o}$
$\hat{r}$	$\frac{r}{r_o}$
r	Radial distance
$\hat{\dot{r}}$	$\frac{\dot{r}}{\dot{r}_o}$
$\dot{r}$	Regression rate of fuel surface
$\hat{R}_i$	$\frac{R_i}{C_{po}}$
R_i	Gas constant of the i^{th} chemical species
Re	Reynolds number, $\frac{r_o \rho_o v_o}{D_o}$
Schmidt Sc	Schmidt number Schmidth number, $\frac{\mu_o}{\rho_o D_o}$
$\hat{t}$	$\frac{t v_o}{r_o}$
t	Time
$\hat{T}$	$\frac{T}{T_o}$

LIST OF SYMBOLS (continued)

T	Temperature of gas mixture
$\hat{T}_s$	$\frac{T_s}{T_{so}}$
T_s	Temperature of solid fuel
UFL	Upper flammability limit
$\hat{v}_r$	$\frac{v_r}{v_o}$
v_r	Radial velocity component
$\hat{v}_z$	$\frac{v_z}{v_o}$
v_z	Axial velocity component
$\hat{W}_i$	$\frac{W_i}{W_o}$
W_i	Rate of production of the i^{th} chemical species per unit volume
y_i	Mass fraction of the i^{th} chemical species
$\hat{z}$	$\frac{z}{r_o}$
z	Axial distance
α	Thermal diffusivity, $\frac{\lambda}{\rho C_p}$
$\hat{\lambda}$	$\frac{\lambda}{\lambda_o}$
λ	Thermal conductivity
$\hat{\mu}$	$\frac{\mu}{\mu_o}$
μ	Viscosity of gas mixture

ν'	Stoichiometric coefficient of reactants
ν''	Stoichiometric coefficient of products
$\hat{\rho}$	$\frac{\rho}{\rho_o}$
ρ	Density of gas mixture

Subscripts

F	fuel
i	The i^{th} chemical species in the gas mixture
Ox	Oxidizer
P	Product
s	The corresponding value for solid fuel
w	The corresponding value at the gas-solid interface
o	The characteristic value

I. INTRODUCTION

The work reported herein represents an extension of the work performed under NASA Contract No. NAS1-10210, Task Order No. 2 [1], following initial work under NASA Grant No. NGR-47-005-085 [2]. The numerical computation was performed on the NASA Langley's CDC 6400/6600 computing facility.

The analytical models have been developed with a view to simulating realistic combustion processes in nonmetalized hybrid rocket systems. In order to check out the numerical computational techniques used, previous calculations had been performed for hybrid rocket systems with axial lengths of 0.36 radius. The purpose of this investigation was to perform further tests on the analytical models, using a more realistic axial length of 3.7 radii. The temperature dependent Arrhenius type fuel regression rate model was chosen for the study.

Again, the Plexiglas-oxygen (PMM-O_2) system was selected for the current study. This allows the order of magnitude for the rate constant of the PMM-O_2 reaction to be estimated from the previous work in reference [1]. Parametric variations of flow rate and chamber pressure were made in an attempt to correlate the published experimental steady-state regression rate data.

In the interior-ballistic design of hybrid rocket systems it is desirable to be able to predict the rate of fuel consumption as a function of axial position and of rate of oxidizer injection. The available steady-state experimental data were tailored towards this end. The steady-state regression rate as a function of axial position at a known oxidizer mass injection rate is, therefore, of prime interest in the current study.

Numerical calculations were performed for six cases, and, profiles of the steady-state regression rate as a function of the axial position were obtained. Instead of an increase in the steady-state regression rate, there was a decrease when the pressure was increased at constant oxygen mass injection rate. Steady-state profiles of flame temperature and mass fraction of the product were analyzed. This adverse effect

is believed to be caused by a layer of cold unburnt mixture of fuel and oxidizer in the immediate vicinity of the fuel surface acting as a heat shield for the fuel surface and thus blocking off the increased heat release from the combustible gas at higher pressure. Recommendations have been made for corrections to vary the chosen inlet conditions and the values for the reaction criteria to eliminate this effect.

It is shown that the flame position in the combustion chamber can be predicted from the calculated results, and that, this type of information can possibly be used for future experimental correlations.

II. ANALYTICAL MODELS

The system under study, as shown in Fig.1, consists of an oxidizer, such as oxygen, flowing through a tubular solid material where chemical reactions take place in the gaseous phase. The fundamental approach has been followed in formulating the analytical models. The mathematical equations derived have been expressed in dimensionless form. Finite rate chemical kinetics and appropriate reaction mechanisms have been incorporated in modelling the gas phase chemical reaction. A temperature dependent Arrhenius type fuel regression rate model has been selected for the current study.

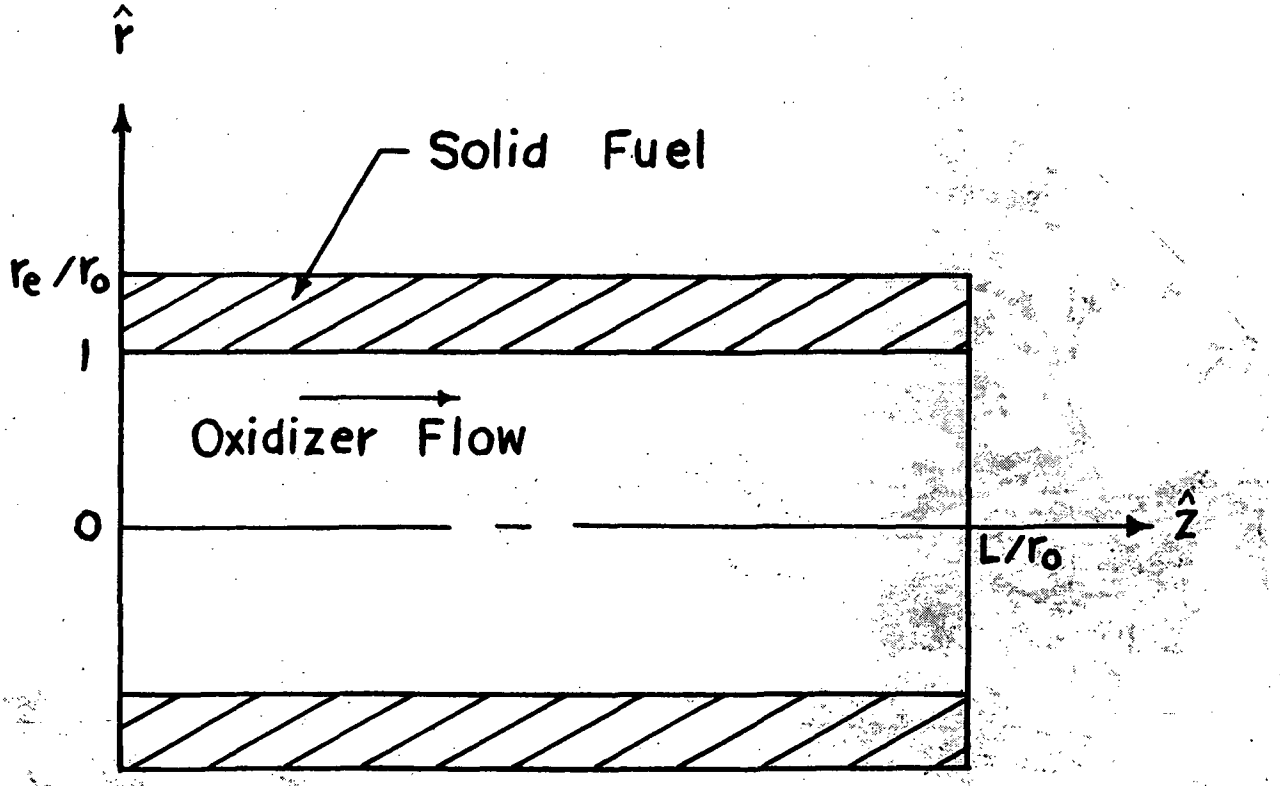

Figure 1. The Physical System

A. Non-Dimensional Equations

The mathematical formulation employs the general time-dependent two-dimensional conservation equations in cylindrical coordinates as the governing equations for the gas phase, the solid phase, and, the gas-solid interface [2]. The governing equations in the gas phase are as follows:

Species Continuity Equations:

$$\hat{\rho}\frac{Dy_i}{DDt} = \frac{1}{ReSc}\left[\frac{\partial}{\partial r}\left(\hat{\rho}\hat{D}_i\frac{\partial y_i}{\partial r}\right) + \left(\frac{\hat{\rho}\hat{D}_i}{r}\right)\left(\frac{\partial y_i}{\partial r}\right) + \frac{\partial}{\partial z}\left(\hat{\rho}\hat{D}_i\frac{\partial y_i}{\partial z}\right)\right] + Da\hat{W}_i, \qquad (1)$$

$$i = 1, 2, \ldots, N$$

Momentum Equations:

$$\hat{\rho}\frac{Dv_r}{Dt} = -\frac{\partial \hat{P}}{\partial r} + \frac{1}{Re}\left\{\frac{2}{3}\frac{\partial}{\partial r}\left[\hat{\mu}\left(2\frac{\partial \hat{v}_r}{\partial r} - \frac{\hat{v}_r}{r} - \frac{\partial \hat{v}_z}{\partial z}\right)\right]\right.$$

$$\left. + \frac{2}{3}\left(\frac{\hat{\mu}}{r}\right)\left(2\frac{\partial \hat{v}_r}{\partial r} - \frac{\hat{v}_r}{r} - \frac{\partial \hat{v}_z}{\partial z}\right) + \frac{\partial}{\partial z}\left[\hat{\mu}\left(\frac{\partial \hat{v}_z}{\partial r} + \frac{\partial \hat{v}_r}{\partial z}\right)\right]\right\}, \qquad (2)$$

$$\hat{\rho}\frac{Dv_z}{Dt} = -\frac{\partial \hat{P}}{\partial z} + \frac{1}{Re}\left\{\frac{\partial}{\partial r}\left[\hat{\mu}\left(\frac{\partial \hat{v}_z}{\partial r} + \frac{\partial \hat{v}_r}{\partial z}\right)\right] + \frac{\hat{\mu}}{r}\left(\frac{\partial \hat{v}_z}{\partial r} + \frac{\partial \hat{v}_r}{\partial z}\right)\right.$$

$$\left. + \frac{2}{3}\frac{\partial}{\partial z}\left[\hat{\mu}\left(2\frac{\partial \hat{v}_z}{\partial z} - \frac{\partial \hat{v}_r}{\partial r} - \frac{\hat{v}_r}{r}\right)\right]\right\},$$

Energy Equation:

$$\hat{\rho}\hat{C}_p\frac{D\hat{T}}{Dt} = Ec\frac{D\hat{P}}{Dt} + \frac{1}{PrRe}\left[\frac{\partial}{\partial r}\left(\hat{\lambda}\frac{\partial \hat{T}}{\partial r}\right) + \frac{\hat{\lambda}}{r}\frac{\partial \hat{T}}{\partial r} + \frac{\partial}{\partial z}\left(\hat{\lambda}\frac{\partial \hat{T}}{\partial z}\right)\right]$$

$$+ \frac{1}{ReSc}\left[\hat{\rho}\frac{\partial \hat{T}}{\partial r}\left(\sum_i \hat{D}_i\hat{C}_{pi}\frac{\partial y_i}{\partial r}\right) + \hat{\rho}\frac{\partial \hat{T}}{\partial z}\left(\sum_i \hat{D}_i\hat{C}_{pi}\frac{\partial y_i}{\partial z}\right)\right]$$

$$\dot{q} = Da\left(\sum_i \hat{h}_i \hat{w}_i\right) \tag{4}$$

Equation of State:

$$\hat{P} = \frac{1}{Ec}\sum_{i=1}^{N} (\gamma_i \hat{R}_i)\hat{\rho}\hat{T} \tag{5}$$

The governing equation in the solid phase is as follows:
Transient Heat Conduction Equation:

$$\hat{\rho}_s C_s \frac{\partial \hat{T}_s}{\partial t} = \frac{\alpha_{so}}{r_o v_o}\left[\frac{\partial}{\partial r}\left(\hat{\lambda}_s \frac{\partial \hat{T}_s}{\partial r}\right) + \left(\frac{\hat{\lambda}_s}{r}\right)\left(\frac{\partial \hat{T}_s}{\partial r}\right) + \left(\frac{\partial}{\partial z}\right)\left(\hat{\lambda}_s \frac{\partial \hat{T}_s}{\partial z}\right)\right] \tag{6}$$

The governing equations derived for the interface are as follows:
Mass Balance:

$$\frac{D_o}{r_o v_o}\left(\frac{\partial y_i}{\partial r}\right)_w \hat{\rho}_w \hat{D}_{iw} - \hat{\rho}_w \hat{v}_w y_{iw} = \left(\frac{\rho_{so}}{\rho_o}\right)\left(\frac{\dot{r}_o}{v_o}\right)\hat{\rho}_s \dot{\hat{r}}\, y_{isw},$$

$$i = 1, 2, \ldots, N \tag{7}$$

Energy Bl
Energy Balance:

$$-\left(\frac{T_{so}}{T_o}\right)\left(\frac{\lambda_{so}}{\lambda_o}\right)\left(\hat{\lambda}_s \frac{\partial \hat{T}_s}{\partial r}\right)_w = \hat{\rho}_w \hat{v}_w \left(\frac{r_o v_o}{\alpha_o}\right)\left[\sum_i (\hat{h}_i y_i)\right] - \left(\hat{\lambda} \frac{\partial \hat{T}}{\partial r}\right)_w$$

$$+ \hat{\rho}_{sw} \dot{\hat{r}} \left(\frac{T_{so}}{T_o}\right)\left(\frac{\lambda_{so}}{\lambda_o}\right)\left(\frac{r_o \dot{r}_o}{\alpha_{so}}\right)\left[\sum_i (\hat{h}_{sgi} y_{isw})\right]$$

$$- \hat{\rho}_w \left(\frac{D_o}{\alpha_o}\right)\left[\sum_i \left(\hat{h}_i \hat{D}_i \frac{\partial y_i}{\partial r}\right)_w\right]. \tag{8}$$

By definition, the sum of the mass fraction of chemical species is equal to unity. Hence, there are only (N-1) independent species

continuity equations. However, in order to eliminate roundoff error in the process of subtraction by computers, N of the species continuity equations were solved.

The complete set of equations should include the continuity equation, however, difficulties with the numerical solutions were experienced when it was included. As an alternative, the set of equations shown above was solved with an initially assumed pressure gradient. Numerical iteration of the pressure gradient should then be performed to obtain the exact solution.

B. Numerical Methods Used

The appropriate finite-difference schemes of second order accuracy have been selected to solve these dimensionless equations numerically. An implicity Lax-Wendroff scheme for the gas phase equations, an implicit Crank-Nicolson scheme for the transient heat conduction equation, and a time-independent finite-difference scheme for the boundary equations have been employed in deriving the difference equations for computer programming. The difference analogs of these finite-difference schemes are presented in reference [3].

Since the numerical schemes employed are implicit, an iterative procedure had to be used. In addition, a relaxation procedure was employed for the purpose of convergence, and, the Aitken's δ^2 method [4] was used as an accelerating convergence procedure during the iterations at each time level to speed up the calculations.

In the current study, the combustion process is dominating. An imposed constant favarable downstream pressure gradient was found sufficient. Hence, no numerical iteration of the pressure gradient has been performed.

C. Reaction Kinetics

Since there is a lack of understanding of the kinetic mechanisms for most of the fuel-oxidizer combinations of interest, a one-step stoichiometric reaction is assumed as follows:

$$\nu_F\ I_F + \nu_{Ox}\ I_{Ox} \xrightarrow{k} \nu_P\ I_P \tag{9}$$

The reaction mechanisms are modeled by two criteria - a critical temperature, T_c, and, the upper and lower limits of flammability (UFL,LFL). Mathematically, these two criteria are as follows:

$$T > T_c \tag{10}$$

$$UFL > \frac{y_F}{y_{Ox}} > LFL \tag{11}$$

When the above two criteria are met locally, the reaction is assumed to occur. The rate of production of species for this overall reaction is calculated as follows:

$$\hat{W}_i = \frac{k M_i}{W_o} (\nu_i'' - \nu_i') \left[I_F\right]^a \left[I_{Ox}\right]^b \tag{12}$$

where a and b are the reaction orders for the fuel and oxidizer respectively.

D. Regression Rate Equation

It has been demonstrated experimentally that the fuel surface regression rate in hybrid rocket systems varies in the axial direction. The regression rate model should allow $\dot{r}$ to be calculated from the input parameters and be used as a combustion model to predict trends in $\dot{r}$ due to operational variables. Hence, the current model assumes that the fuel surface chemical reaction is a function of the local temperature at the gas-solid interface, T_w, such that the fuel surface regression rate can be expressed in the Arrhenius form as follows:

$$\dot{r} = A_s \exp\left[\frac{E_s}{R\ T_w}\right] \tag{13}$$

where A_s and E_s are empirical constants.

III. NUMERICAL CALCULATIONS

The hybrid rocket motor selected for the current analytical study has the following dimensions: r_o = 2.54 cm (1.0 in), r_e = 2.56 cm (1.007 in), and, L = 9.408 cm (3.70 in). For the current study, six sets of calculations were performed with pre-selected values of flow rate and chamber pressure.

A. Selection of Fuel and Oxidizer

Plexiglas (PMM) and oxygen (O_2) have been selected as the fuel and the oxidizer for the current study, because our previous work [1], allows us to pick the correct magnitude for the rate constant in modelling the PMM-O_2 reaction through parametric variation of the rate constant. In addition, the PMM-O_2 combination is a relatively simple system which can readily be simulated in an experimental program.

B. Initial and Boundary Conditions

The initial and boundary conditions used were as follows:

(a) A fully-developed flow of pre-heated oxygen (1620° R) reaching the inlet of the combustion chamber, such that the axial component of the velocity distribution at the inlet is based on the (1/7)-power law for turbulent flow, i.e.,

$$\hat{v}_z = (1 - \hat{r})^{1/7}; \qquad (14)$$

(b) The assumed initial temperature profile represents the conditions at the start of the ignition process;

(c) The temperature at the exterior surface of the solid fuel is constant;

(d) The axial component of velocity is zero at the gas-solid interface and the radial component of velocity is zero at the center line.

C. Reaction Kinetics

Since there is a lack of understanding of the kinetic mechanism for the PMM-O_2 reaction, a one-step stoichiometric reaction is assumed as follows:

$$C_5H_8O_2 + 6O_2 \xrightarrow{k} 5CO_2 + 4H_2O \qquad (15)$$

In order to save computer time, the reaction products CO_2 and H_2O are treated as one single species such that the reaction can be represented as follows:

$$C_5H_8O_2 + 6O_2 \xrightarrow{k} 9 \text{ Product} \qquad (16)$$

where the product is a mixture containing 5 parts of gaseous carbon dioxide and 4 parts of water vapor.

Treating the overall reaction of PMM and O_2 in the same manner as in reference [1], an order-of-magnitude value for the rate constant was estimated for the current study. This selected value was

$k = 3.9 \times 10^{16}$ cm^6/g-mole^2/sec (10^{13} ft^6/lb$_m$-mole^2/sec).

D. Property Models

The models for the transport properties, the fluid properties and the properties for the solid fuel were assumed to be constant in the same manner as reported in reference [2]. The property values were estimated if they were not readily available. The selected thermophysical properties for PMM, O_2 and the product were obtained either directly or by estimations from references [5] through [9] and are tabulated in Table I. Following the approach outlined in reference [2], equivalent turbulent values were used for the transport properties. These selected values are μ = 0.00893 g/cm/sec (0.0006 lb$_m$/sec/ft), D_i = 8.23 cm^2/sec (0.00886 ft^2/sec), and λ = 0.0031 cal/sec/cm/°K (0.75 Btu/hr/ft/°R).

TABLE I

Selected Thermophysical Properties for Plexiglas (PMM), Oxygen and the Product*

	PMM	O_2	Product*
M_i, g/g-mole, or, lb_m/lb_m-mole	100.0 [5]	32.0 [5]	32.4 [5]
C_p, cal/g/°k, or, $Btu/lb_m/°R$	0.35 [6]	0.25 [7]	0.20 [7]
$h°$, cal/g	- 928	0	2601.7
$h°$, Btu/lb_m	-1670 [8]		-4680.0 [5]
Boiling point, °K	374	90.19	373.3
Boiling point, °R	673.2 [8]	162.34 [5]	672.0 [5]
$h_{s\ell}$, † cal/g	130	-	-
$h_{s\ell}$, † Btu/lb_m	234 [8]		
h_L †† cal/g	86	-	133.4
$h_{\ell g}$, †† cal/g	86		
$h_{\ell g}$, †† Btu/lb_m	155 [8]		240.0 [5]
ρ_s, g/cm^3	1.683	-	-
ρ_s, lb_m/ft^3	150 [6]		
λ_s, cal/sec/cm/°K	0.0012	-	-
λ_s, Btu/hr/ft/°R	0.289 [6]		
C_s, cal/g/°K, or, $Btu/lb_m/°R$	0.31 [9]		

*A mixture containing 5 parts of gaseous carbon dioxide and 4 parts of water vapor.

†heat of fusion

††heat of vaporization

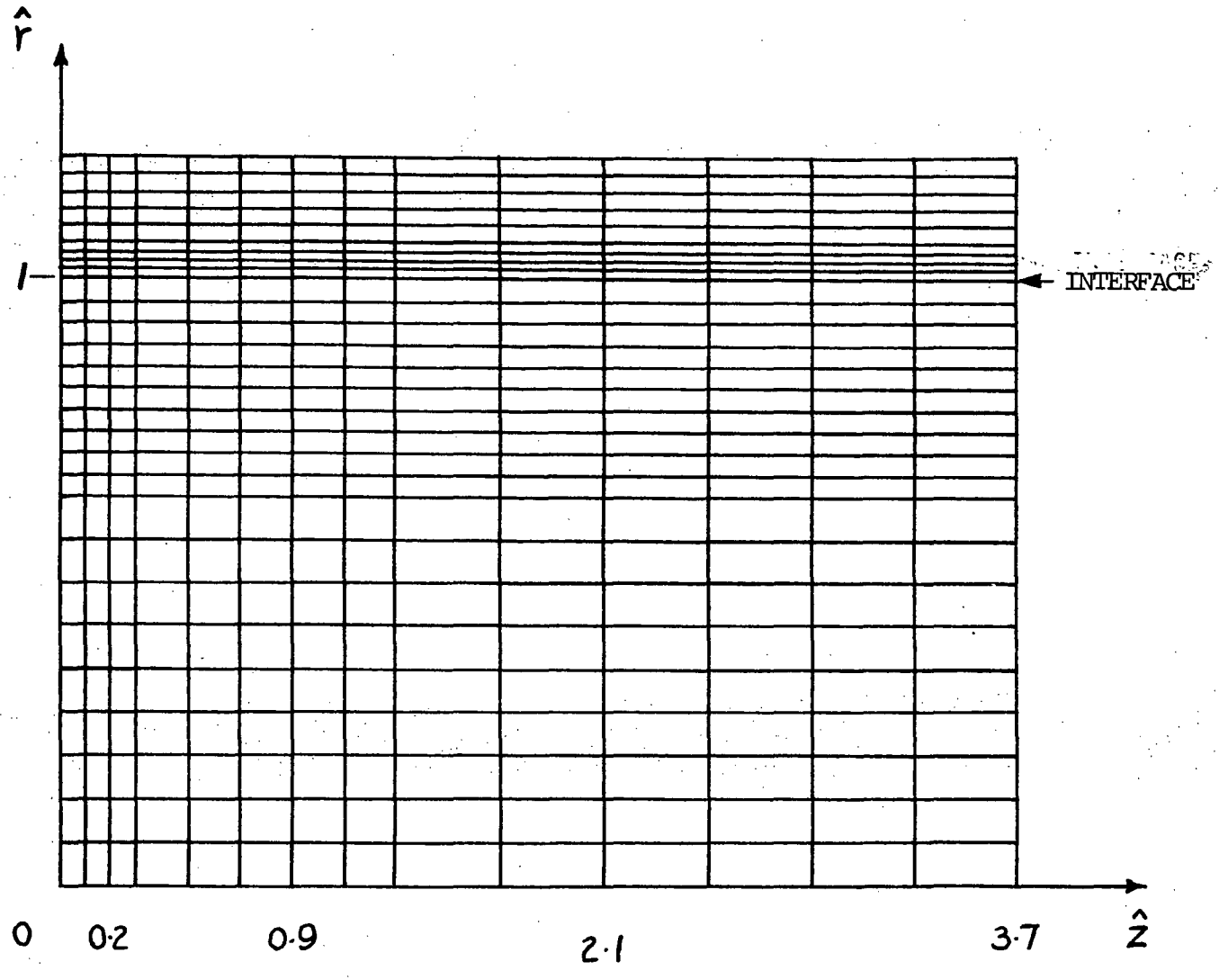

Figure 2. Grid Layout

E. Imposed Pressure Gradient

In order to obtain numerical solution, a constant favorable downstream pressure gradient equal to that used by Jones and Issaacson [10] in their analysis was imposed as in reference [2]. This imposed pressure gradient is

$$-\frac{dP}{dz} = 2.576 \text{ dyne/cm}^2\text{/cm} \quad (0.164 \text{ psf/ft}). \tag{17}$$

F. Grid Layout

The grid layout selected for the numerical calculations is shown is Fig. 2. There were 15 stations along the axis in the z direction. The ratio of the grid size for the three uniformly spaced regions in the axial direction was 1:2:4. In the r direction, there were 20 stations in the gas phase and 10 stations in the solid phase. Finer grid size (7:1 for the gas phase and 1:5 for the solid phase) was employed near the gas-solid interface.

G. Empirical Constants for the Regression Rate Equation

A trial and error method as discussed in reference [11] was used to determine the values for the empirical constants A_s and E_s such that $\dot{r}$ = 0.254 mm/sec (0.01 in/sec) at T_w = 644.4° K (1160° R), the initially assumed temperature value at the fuel surface. These numerically determined values are

$$A_s = 0.645 \text{ mm/sec} \quad (0.00211 \text{ ft/sec}) \tag{18}$$

$$E_s = 1.0 \text{ Kcal/g-mole} \quad (1799 \text{ Btu/lb}_m\text{-mole}). \tag{19}$$

H. Parametric Values Used

Numerical calculations were performed for six cases with various values of flow rate and chamber pressure. A compendium of the parametric values used for the numerical calculations of the six cases is shown in Table II.

Table II

Parametric Values Used for the Numerical Calculations

Case	V_o		G_o		P
	m/sec	ft/sec	$g/cm^2/sec$	$lb_m/in^2/sec$	atm
1	32.92	1080	18.98	0.27	1.67
2	36.58	120	6.32	0.09	5.0
3	109.7	360	18.98	0.27	5.0
4	329.2	1080	56.94	0.81	5.0
5	36.58	120	18.98	0.27	15.0
6	109.7	360	56.94	0.81	15.0

IV. RESULTS AND DISCUSSIONS

In performing the numerical calculations, both the transient and the steady-state results have been obtained, the transient solutions provide the guideline in determining when steady-state conditions have been reached. In general, the total time necessary for the transient solution to reach steady-state is approximately twice the time required for the oxidizer at the inlet to reach the axial station being considered.

Since no transient experimental data on this type of system is available, analyses were made primarily on the steady-state results. Hence, only the steady-state solutions are included to illustrate the combustion induced variations in flame temperature, species mass fraction, and regression rate profile as a function of input parameters.

In all the six cases calculated, the initially assumed profiles for the dependent variables, $\hat{v}_r$, $\hat{v}_z$, $\hat{T}$, $\hat{T}_s$, $\hat{\rho}$, Y_{PMM}, and, Y_{O_2} at any axial station are shown in Figures 3a-g, respectively. Initially, the mass fraction of the product was assumed to be zero everywhere.

Holding the pressure constant at 5 atmospheres, the steady-state regression rate for cases 2, 3 and 4 (see Table II) are plotted in Figure 4. It can be observed that an increase in flow velocity at constant pressure, or, in other words, an increase in the mass flow rate of oxygen at the inlet tends to increase the steady-state regression rate. Similar trends were observed at a constant pressure of 15 atmospheres, i.e., cases 5 and 6.

The steady-state regression rate was found to be independent of pressure at flow velocity values of 109.7 m/sec (360 ft/sec) and 329.2 m/sec (1080 ft/sec). This is illustrated by plotting the steady-state regression rate of cases 3 and 6 at constant flow velocity of 109.7 m/sec (360 ft/sec) as shown in Figure 5. However, at lower flow velocity of 36.58 m/sec (120 ft/sec), an increase in pressure tends to increase the steady-state regression rate. This is demonstrated in Figure 6.

With the oxygen mass injection rate held at a constant value of 18.98 $g/cm^2/sec$ (0.27 $lb_m/in^2/sec$), the steady-state regression rate profiles of cases 1, 3 and 5 are plotted in Figure 7. It is observed that an increase in pressure at constant oxygen mass injection rate tends to decrease the steady-state regression rate. The same behavior was observed for cases 4 and 6 when the oxygen mass injection rate was held at a constant value of 56.94 $g/cm^2/sec$ (0.81 $lb_m/in^2/sec$). However, Marxman, Woolridge and Muzzy [11], in their experimental study of PMM-O_2 systems, observed an increase in the steady-state regression rate at higher pressure. In addition, this same effect was reported by Smoot and Price [12] in their experimental study of nonmetalized hybrid fuel systems using three different binder compounds (Butyl rubber, PBAA and Polyruethane) with oxidizers varied from 100% fluorine to 100% oxygen. Hence, the current analytical results do not confirm their experimental observations. The scattered experimental data shown in Reference [11] for PMM-O_2 systems at atmospheric pressure are shown in the cross-hatched region in Figure 8. For comparison, the steady-state regression rate values at axial station 14 for the six cases calculated are plotted in Figure 8.

Steady-state profiles of flame temperature and mass fraction of the product for the six cases calculated were reviewed. It was observed that an increase in pressure at constant oxidizer mass injection rate did increase the flame temperature considerably as shown in Figures 9a-b, and the mass fraction of the product as shown in Figures 10a-b. However, from these figures, it was also observed that the gas-phase combustion did not sustain itself at the radial station next to the fuel surface. This layer of cold unburnt gas mixture decoupled the heating effect on the fuel surface from the combustion zone. As a result, the calculated steady-state regression rates did not display the correct kinetically controlled effect, i.e., an increase in the steady-state regression rate with an increase in pressure.

With the proper choice of the profiles of the mass fraction of fuel and oxidizer at the inlet such that it is less fuel rich at radial station

next to the fuel surface, and, with values for the reaction criteria such that combustion can sustain itself at the radial station next to the fuel surface, it is believed that the correct pressure effect at constant oxidizer mass injection rate should result.

The current analytical method also provides the capability of predicting the position of the flame in the combustion chamber. To demonstrate this point, the peak of the temperature profile was taken as the flame position, and, the steady-state flame position in the combustion chamber for case 3 was predicted as shown in Figure 11. Using Schlieren and shadowgraph techniques, Muzzy [13] was able to predict experimentally the steady-state flame position in a slab burner. The analytical prediction is in qualitative agreement with Muzzy's experimental results. Hence, it is believed that this type of technique can possibly be used for future experimental correlations.

V. CONCLUSIONS AND RECOMMENDATIONS

The computer program developed under NASA Contract No. NAS1-10210, Task Order No. 2 following initial work under NASA Grant No. NGR-47-005-085 for the study of transient combustion processes in hybrid rocket systems has been modified to allow a study of systems with a more realistic axial length (3.7 r_o). Current emphasis has been placed on correlating the calculated steady-state regression rate results with published experimental data. The following has been achieved:

(a) The computer program can now handled a more realistic axial length (3.7 r_o) with reasonable usage of computing time.

(b) The steady-state regression rate at constant pressure increases with increased oxidizer mass injection rate.

(c) The computed steady-state regression rate at constant oxidizer mass injection rate decreased with increased pressure which is in constrast with reported experimental observations. More work is required to investigate these results, which appear to be incorrect.

(d) The steady-state results can possibly be used to predict the flame position in the combustion chamber.

A list of recommendations is as follows:

(a) The inlet mass fraction of fuel and oxidizer at radial station next to the fuel surface and values for the reaction criteria should be varied such that combustion can sustain itself at radial station next to the fuel surface further downstream.

(b) Concurrent analytical and experimental work should be performed to confirm the validity of the current analytical models.

REFERENCES

1. Hung, W.S.Y., Chen, C.S. and Haviland, J.K., "Analytical Study of Hybrid Rocket Combustion," Research Laboratories for the Engineering Sciences, University of Virginia, Report No. ME-4027-103-72U, Prepared under NASA Contract No. NASI-10210, Task Order No. 2, February 1972.

2. Haviland, J.K., Chen, C.S., and Hung, W.S.Y., "Theoretical Study of Reactive Fluid Flow in Heterogeneous Combustion Processes," University of Virginia, Research Laboratories for the Engineering Sciences Report No. AEEP-4007-108-70U (Ph.D. Dissertation, W.S.Y. Hung), under NASA Grant No. NGR-47-005-085, January 1971.

3. Hung, W.S.Y., Chen, C.S. and Haviland, J.K., "Numerical Solutions of Reactive Fluid Flows During Postignition Transients in Hybrid Rocket Systems," Journal of Computational Physics, Vol. 9, pp. 167-193, April 1972.

4. Henrici, P., Elements of Numerical Analysis, John Wiley and Sons, Inc., 1964.

5. Hodgman, D.C., R.C. West and S.M. Selby (eds.), "Handbook of Chemistry and Physics (42nd ed.)," The Chemical Rubber Publishing Co., Ohio, 1960.

6. Saraniero, M.A., L.H. Caveny and M. Summerfield, "Combustion Anomalies in Stop-Restart Firing of Hybrid Rocket Engines," Princeton University, Aerospace and Mechanical Sciences Report No. 945 under NASA Grant No. NGR-31-001-109, September 1970.

7. Obert, E.F., "Concepts of Thermodynamics," p. 494, McGraw-Hill, New York, 1960.

8. "Investigation of Fundamental Phenomena in Hybrid Propulsion," United Technology Center, Final Technical Report (UTC 2097-FR), Vol. I, under Bureau of Naval Weapons Contract No. W64-0659-C, November 1965.

9. Warfield, R.W. and M.C. Petree, "Thermodynamic Properties of Polymethyl Methacrylate and Methyl Methacrylate," NOLTR 62-98, United States Naval Ordnance Lab., White Oak, Maryland, 1962.

10. Jones, J.W. and L.K. Isaacson, "A Turbulent Boundary Layer with Mass Addition, Combustion and Pressure Gradients," AFOSR 70-1428TR, 1970.

11. Marxman, G.A., Wooldridge, C.E. and Muzzy, R.J., "Fundamentals of Hybrid Boundary-Layer Combustion," in Progress in Astronautics and Aeronautics and Aeronautics: Heterogeneous Combustion, pp. 485-522, Academic Press: New York, 1964.

12. Smoot, L.D. and Price, C.F., "Regression Rates of Nonmetalized Hybrid Fuel Systems," AIAA Journal, Vol. 3, No. 8, pp. 1408-1413, 1965.

13. Muzzy, R.J., "Schlieren and Shadowgraph Studies of Hybrid Boundary Layer Combustion," AIAA Journal, Vol. 1, pp. 2159-2160, 1963.

APPENDIX

FIGURE (3a)

INITIAL PROFILE IN GAS PHASE

PMM - O_2

○ $\hat{z}$ = 0.0

□ $\hat{z}$ > 0.0

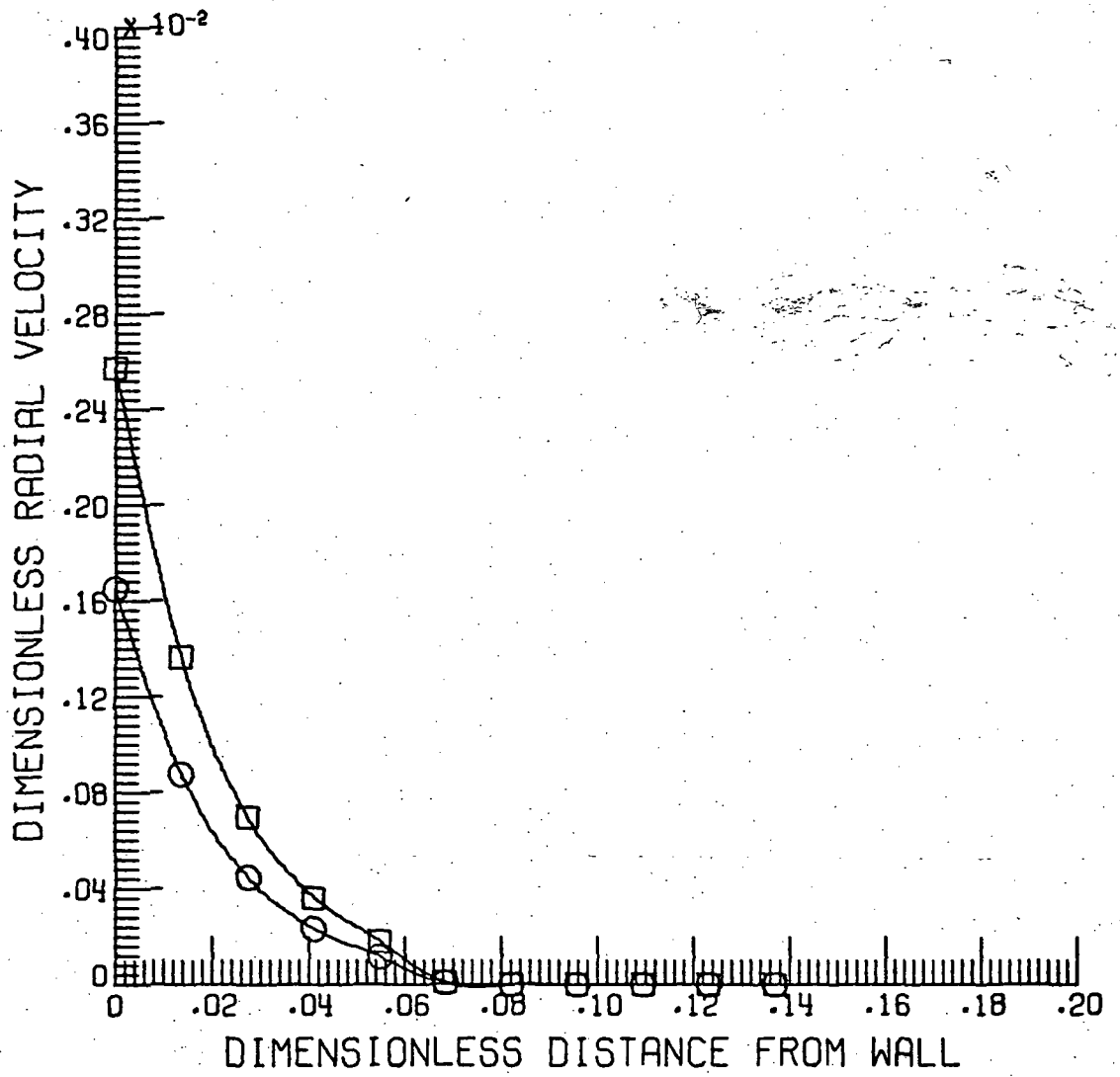

FIGURE (3b)
INITIAL PROFILE IN GAS PHASE

PMM - O_2

○ $\overset{\Delta}{Z}$ = 0.0
□ $\overset{\Delta}{Z}$ > 0.0

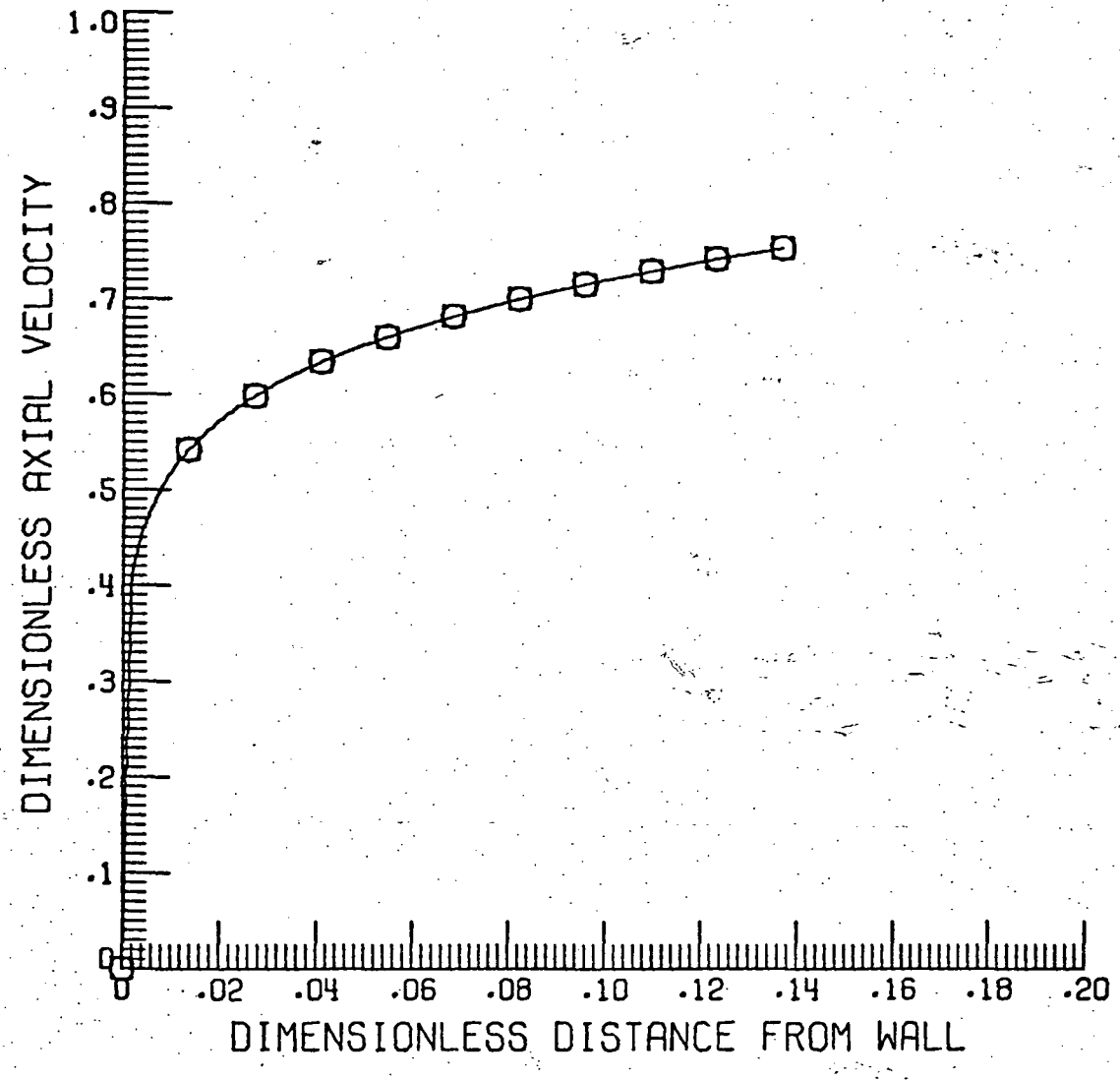

FIGURE (3c)

INITIAL PROFILE IN GAS PHASE

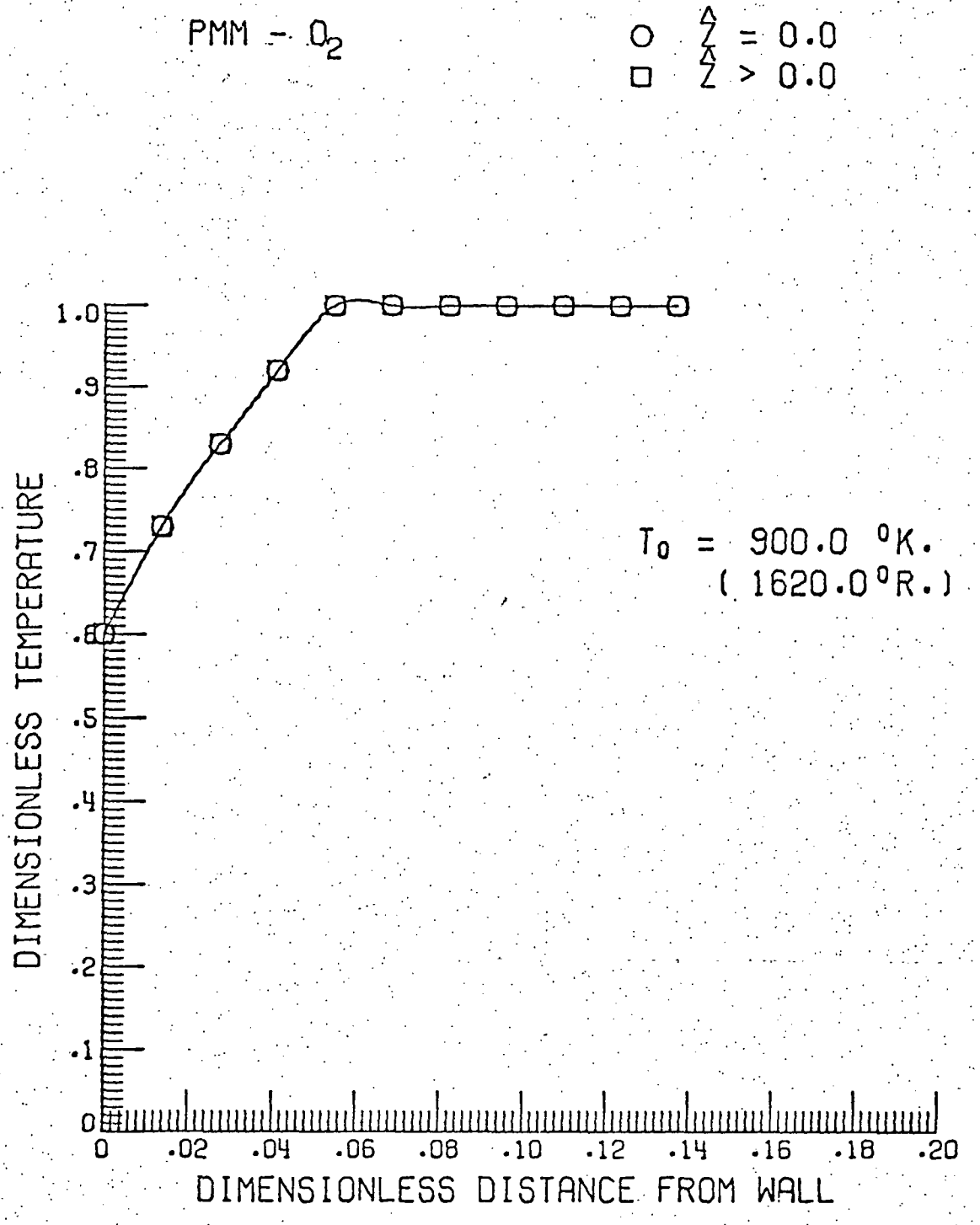

FIGURE (3d)

INITIAL PROFILE IN SOLID PHASE

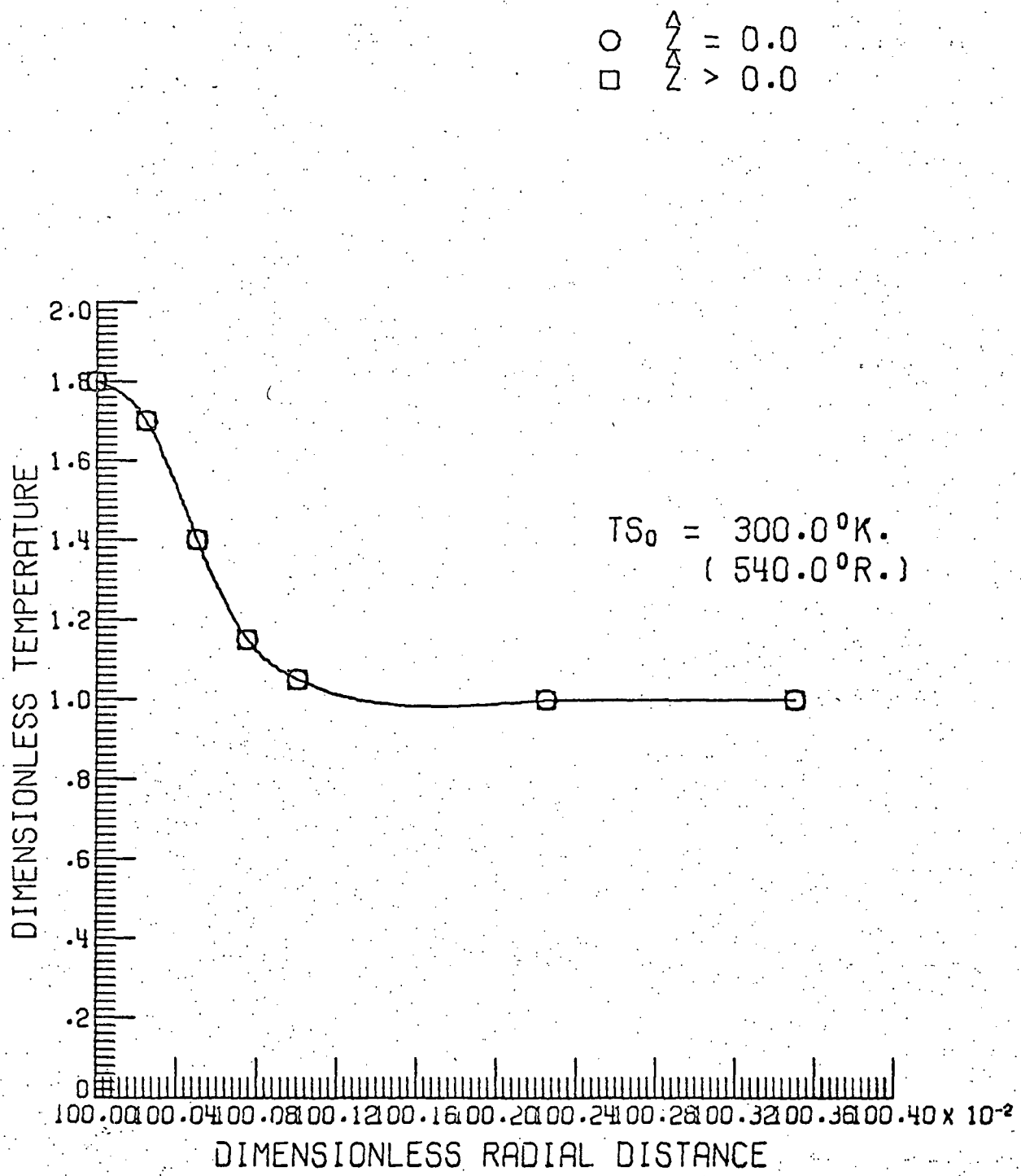

FIGURE (3e)

INITIAL PROFILE IN GAS PHASE

PMM - O_2

○ $\hat{Z}$ = 0.0

□ $\hat{Z}$ > 0.0

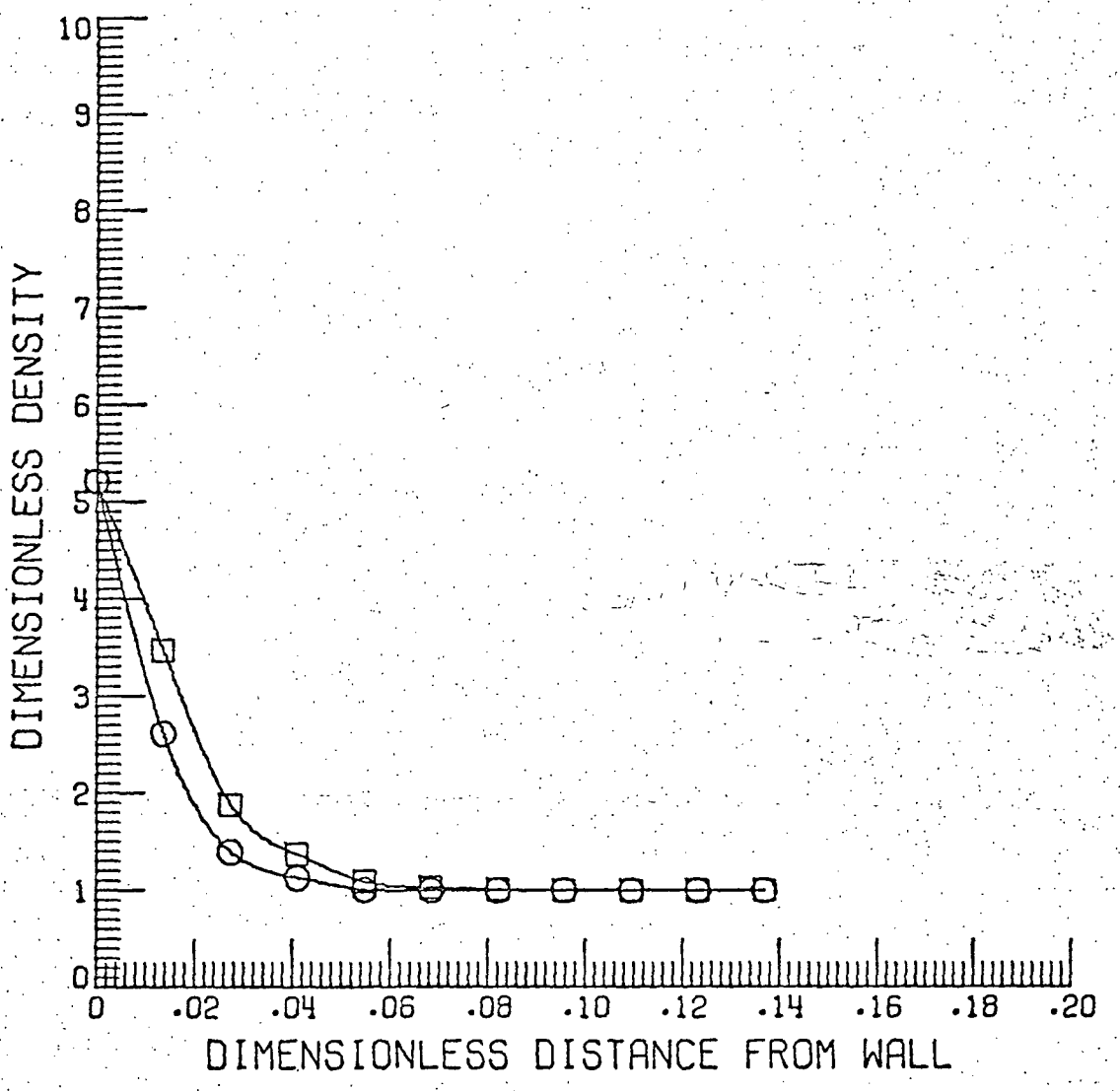

FIGURE (3f)
INITIAL PROFILE IN GAS PHASE

PMM - O_2

○ $\hat{Z} = 0.0$
□ $\hat{Z} > 0.0$

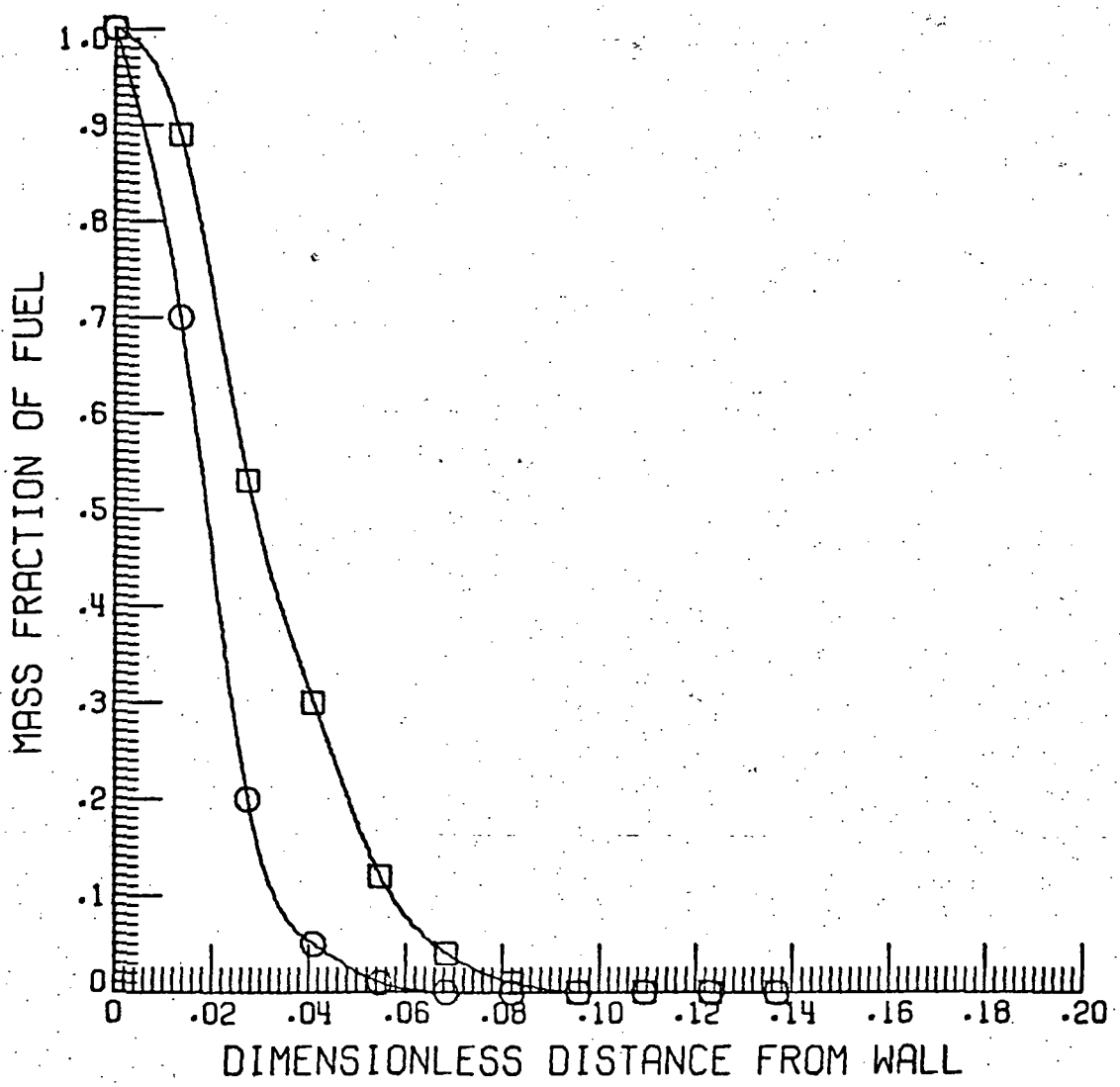

FIGURE (3g)

INITIAL PROFILE IN GAS PHASE

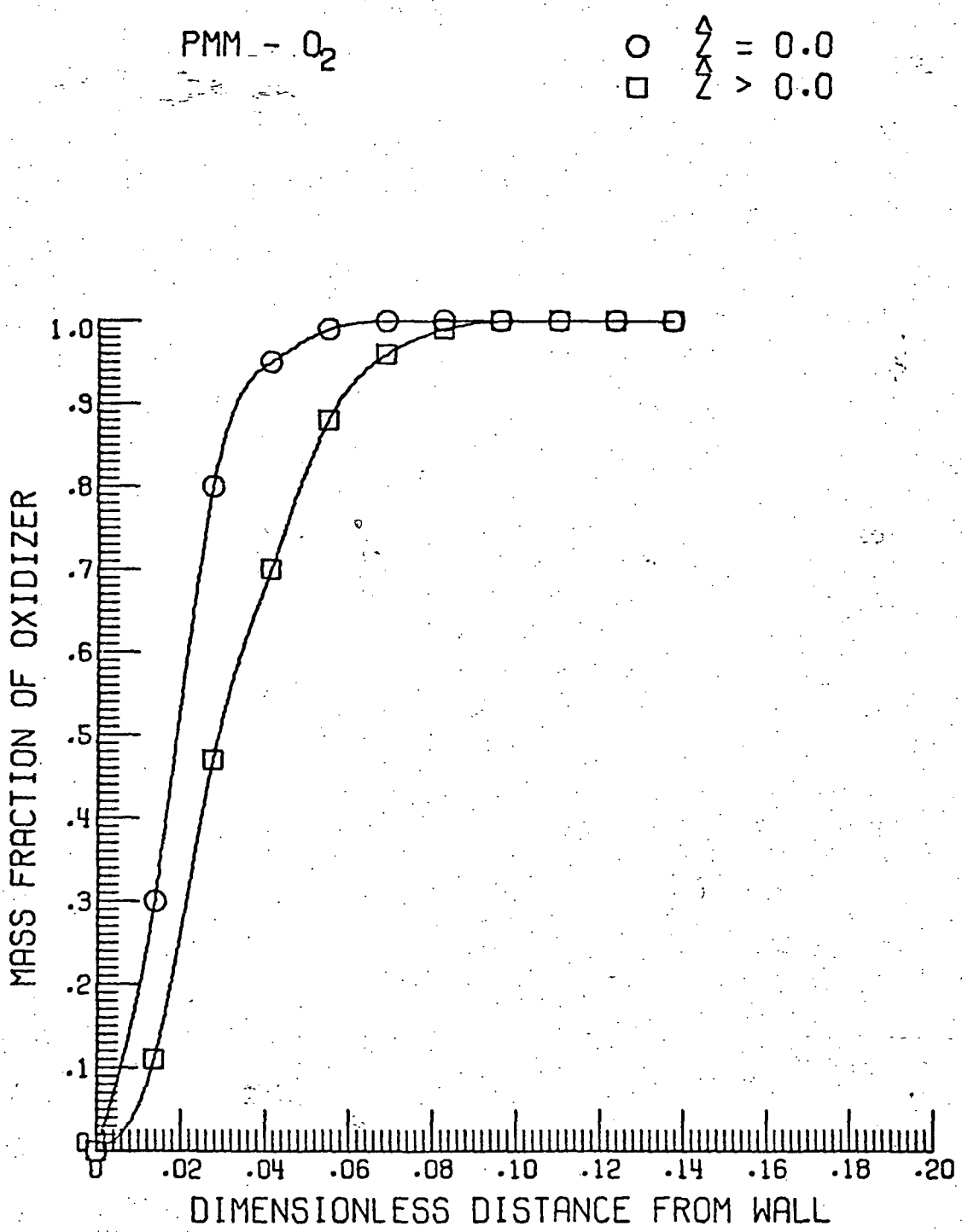

FIGURE (4)

PMM - O_2

2 ○ G_0 = 6.32 GM/SQ.CM-SEC
V_0 = 36.5 M/SEC

3 □ G_0 = 18.98 GM/SQ.CM-SEC
V_0 = 109.7 M/SEC

4 ◇ G_0 = 56.94 GM/SQ.CM-SEC
V_0 = 329.1 M/SEC

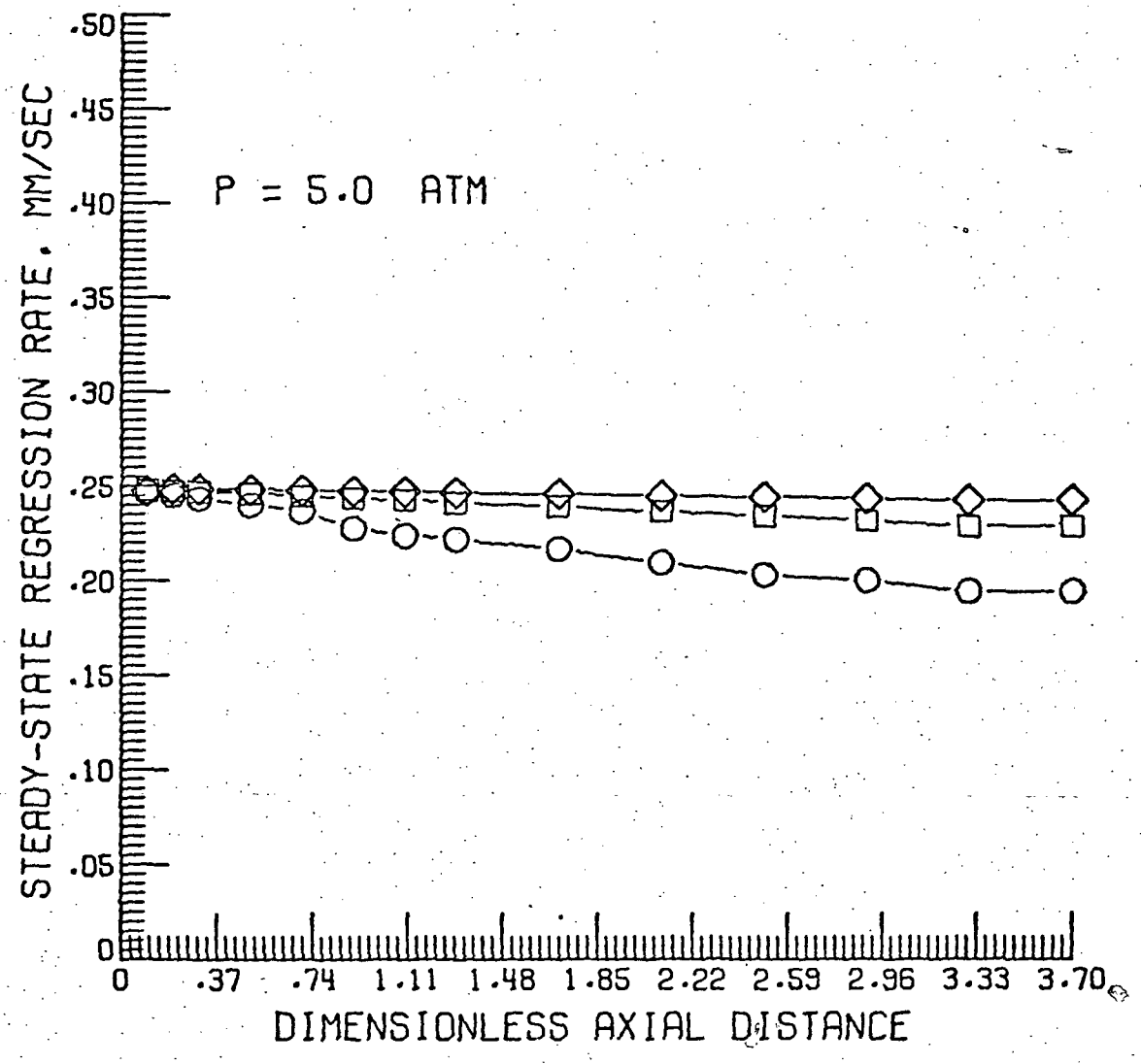

FIGURE (5)

PMM - O_2

6 ○ P = 15.0 ATM
G_0 = 56.9 GM/SQ.CM-SEC

3 □ P = 5.0 ATM
G_0 = 18.9 GM/SQ.CM-SEC

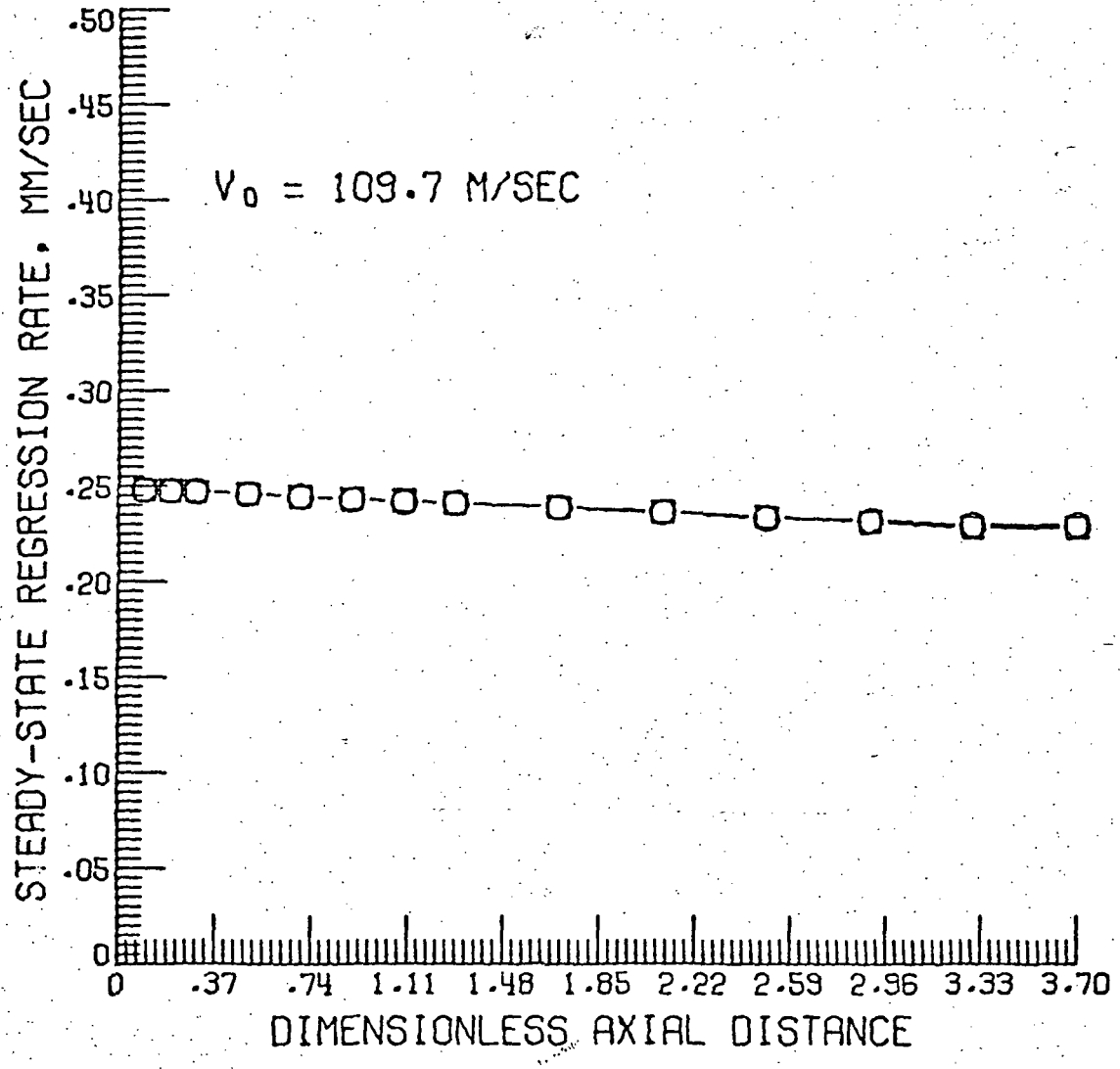

FIGURE (6 6)

PMM - O_2

5 ○ P = 15.0 ATM
G_0 = 18.9 GM/SQ.CM-SEC

2 □ P = 5.0 ATM
G_0 = 6.3 GM/SQ.CM-SEC

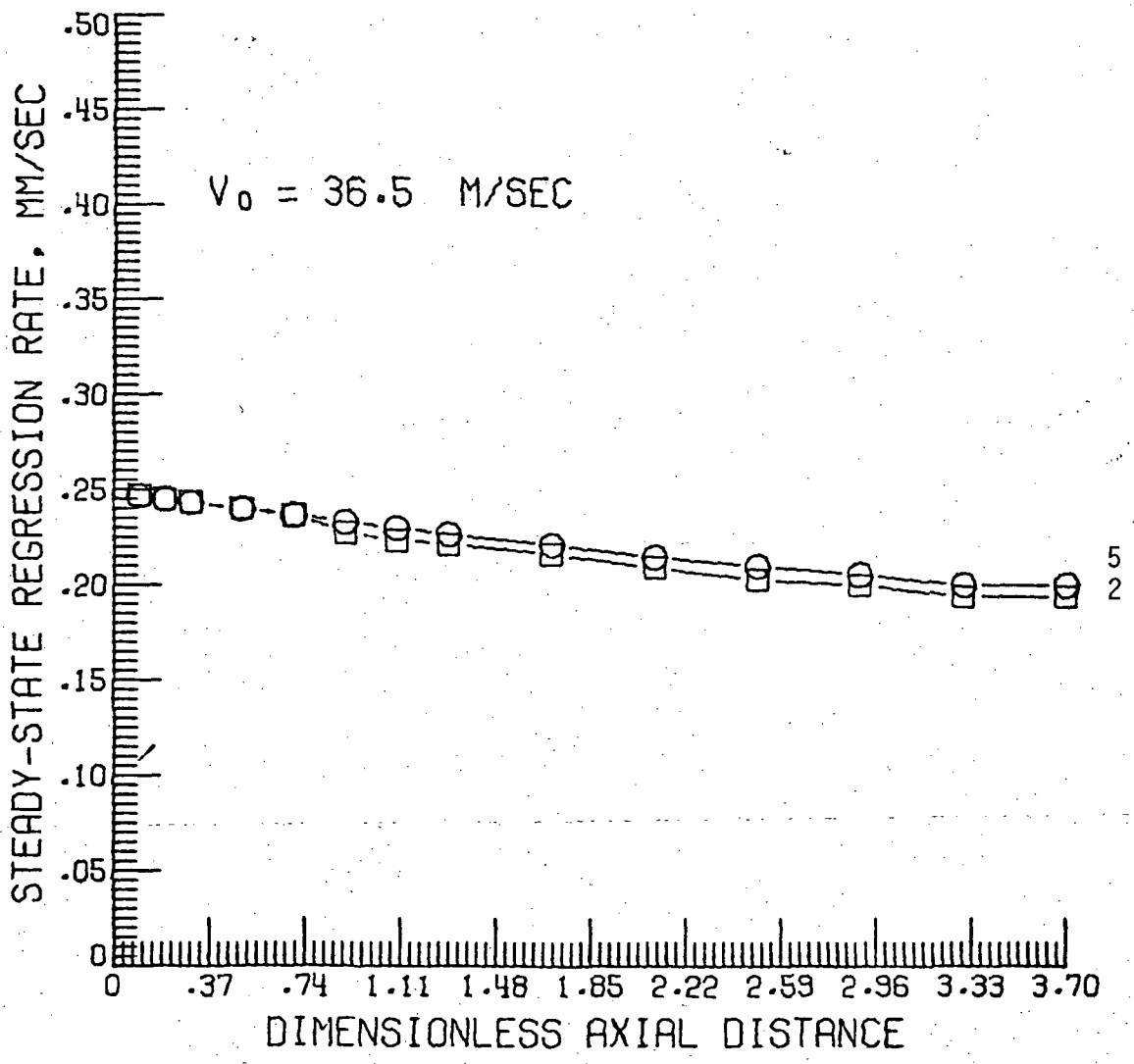

FIGURE (7)

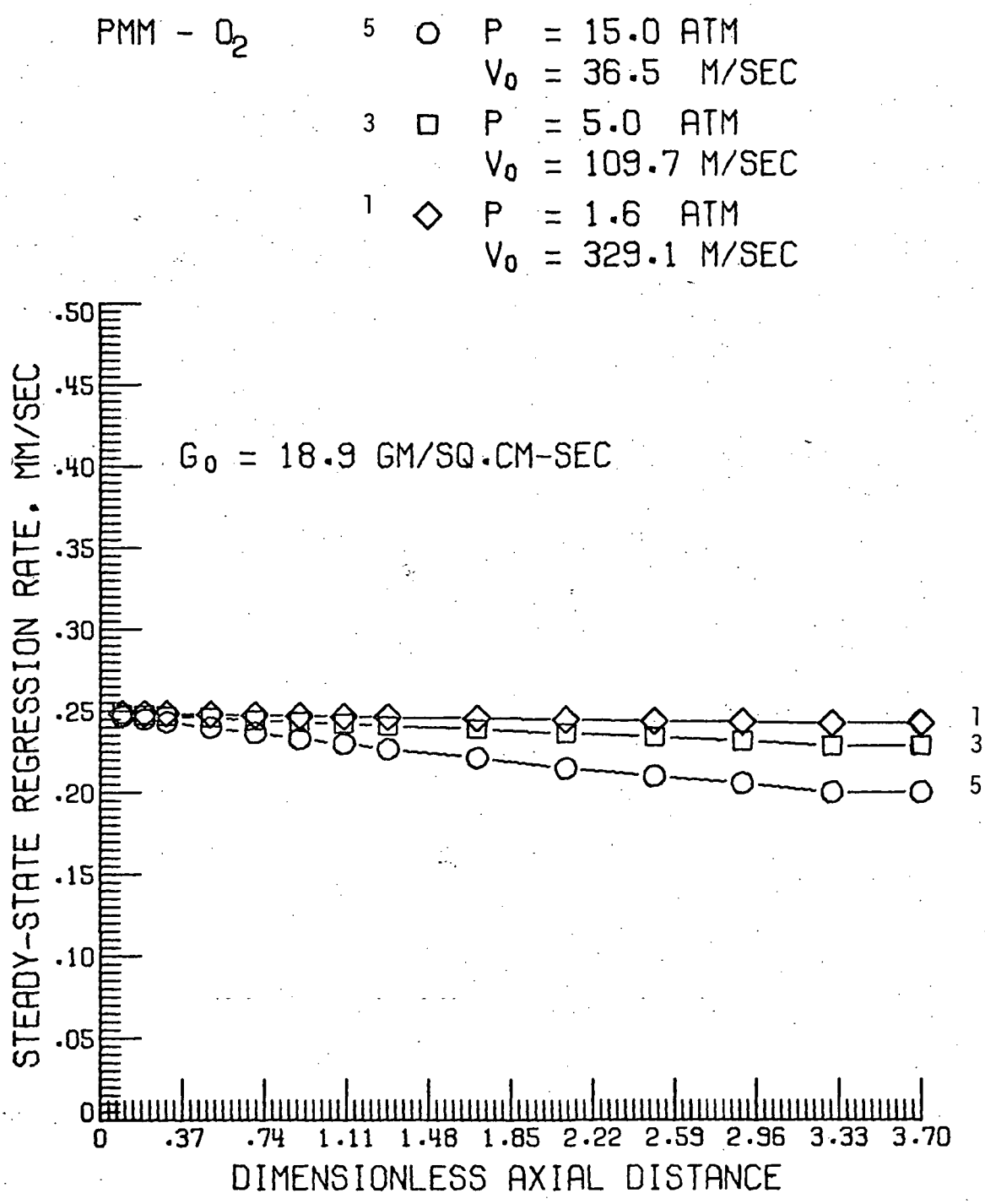
PMM - O_2
5 ○ P = 15.0 ATM
V_0 = 36.5 M/SEC
3 □ P = 5.0 ATM
V_0 = 109.7 M/SEC
1 ◇ P = 1.6 ATM
V_0 = 329.1 M/SEC
G_0 = 18.9 GM/SQ.CM-SEC
STEADY-STATE REGRESSION RATE, MM/SEC
.50
.45
.40
.35
.30
.25
.20
.15
.10
.05
0
0 .37 .74 1.11 1.48 1.85 2.22 2.59 2.96 3.33 3.70
DIMENSIONLESS AXIAL DISTANCE
1
3
5

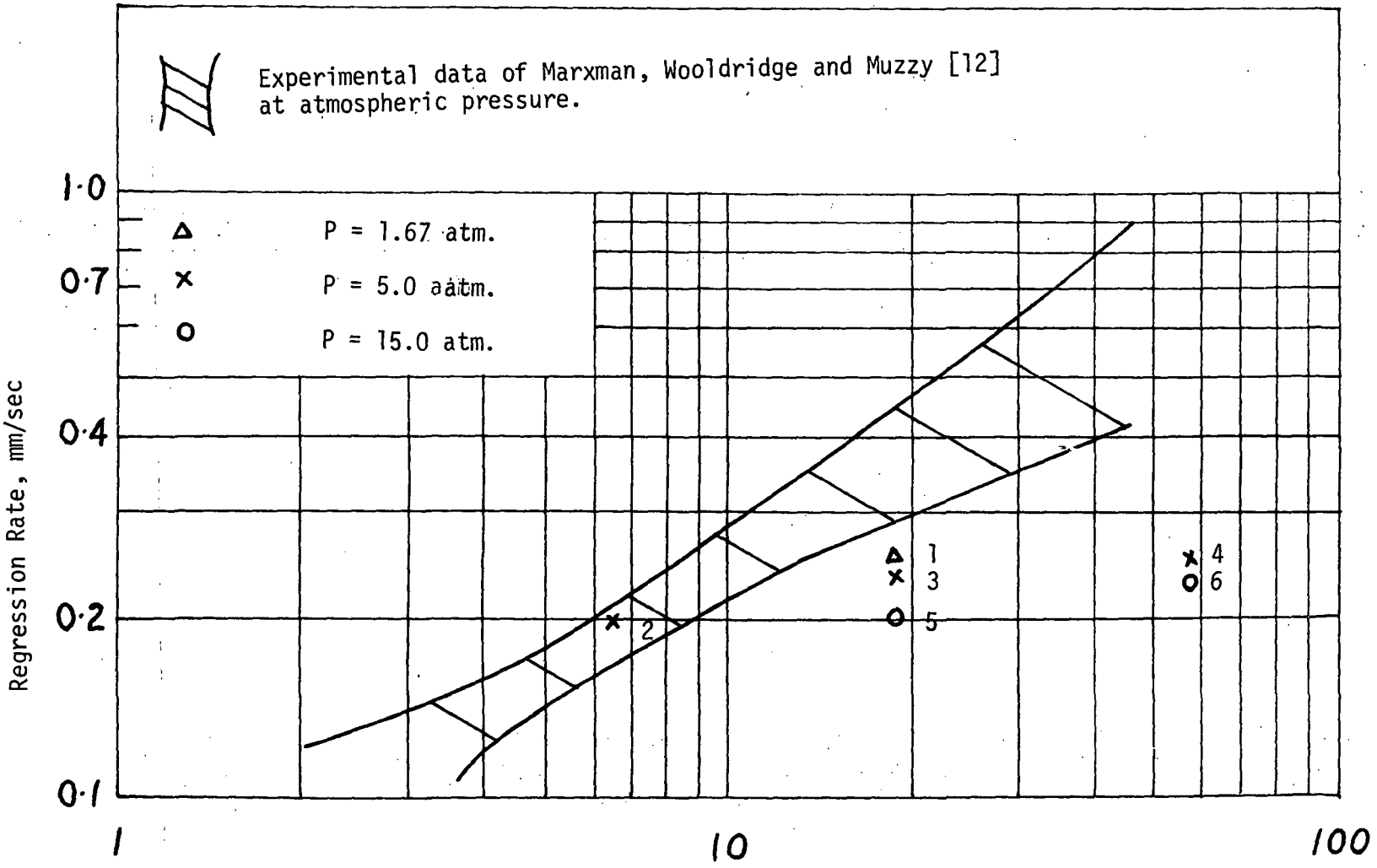

Figure 8. Regression Rate Versus Oxygen Mass Injection Rate for PMM-O_2 Systems.

FIGURE (9a)

PROFILE AT TIME = .00169 SEC.

IN GAS PHASE

PMM - O_2

Case 3

P = 5 atm.

○ Z = 0.00

□ Z = .20

◇ Z = .90

△ Z = 2.10

◺ Z = 3.70

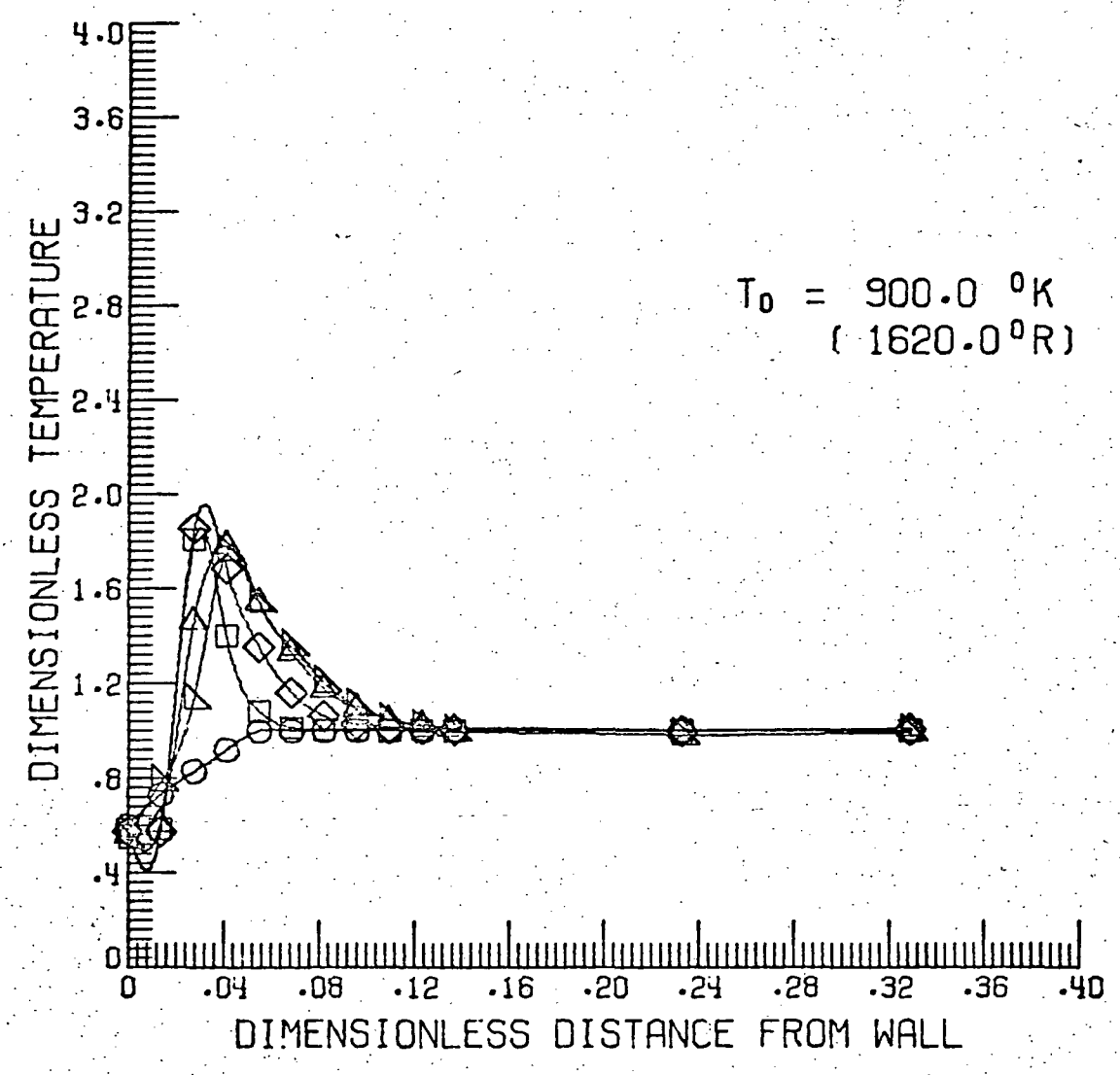

T_0 = 900.0 ^{0}K

(1620.0 ^{0}R)

FIGURE (9b)

PROFILE AT TIME = .00508 SEC.

IN GAS PHASE

PMM - O_2

Case 5

P = 15 atm.

○ Z = 0.00

□ Z = .20

◇ Z = .90

△ Z = 2.10

◺ Z = 3.70

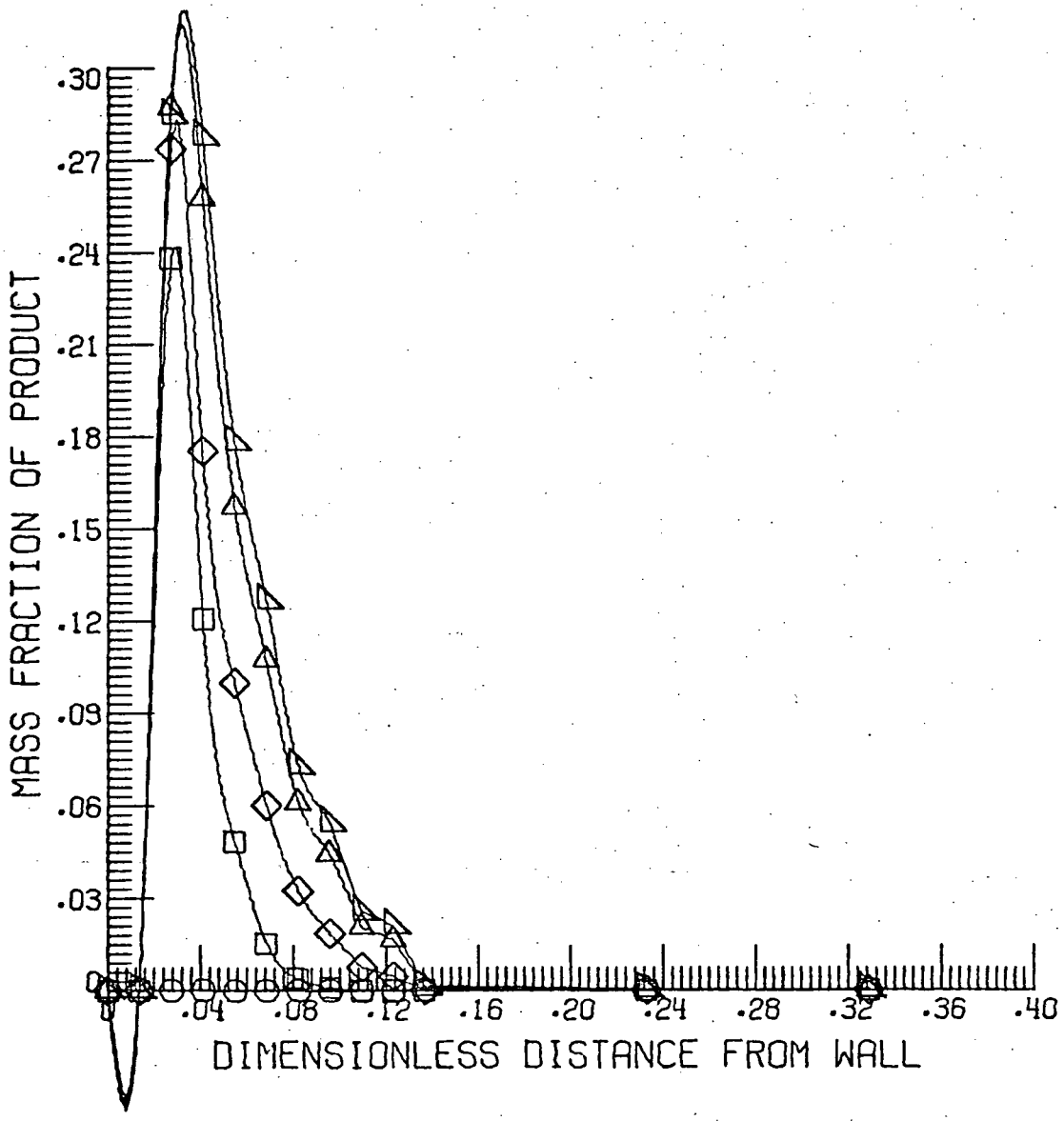

FIGURE (10a)

PROFILE AT TIME = .00169 SEC.

IN GAS PHASE

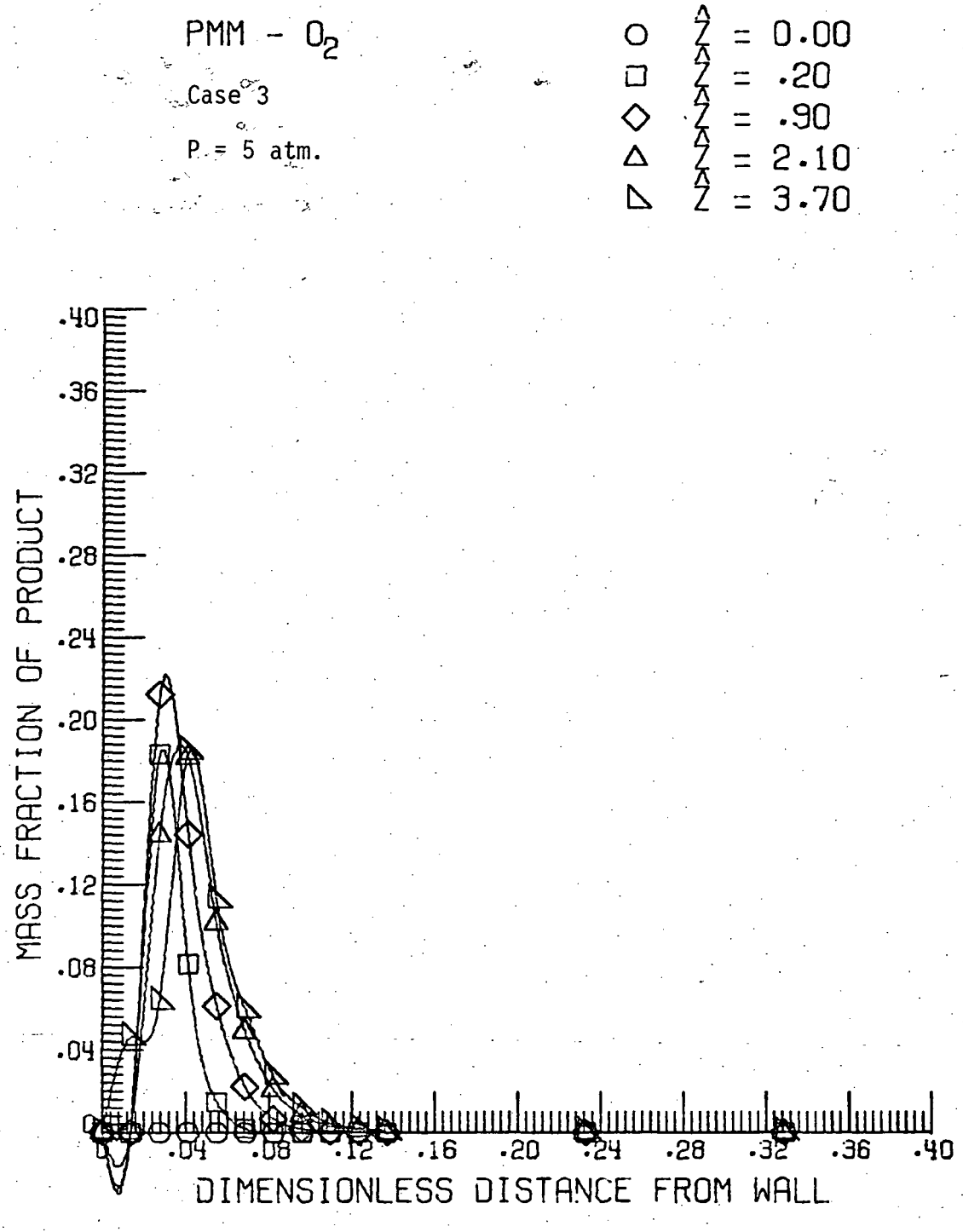

FIGURE (10b)

PROFILE AT TIME = .00508 SEC.

IN GAS PHASE

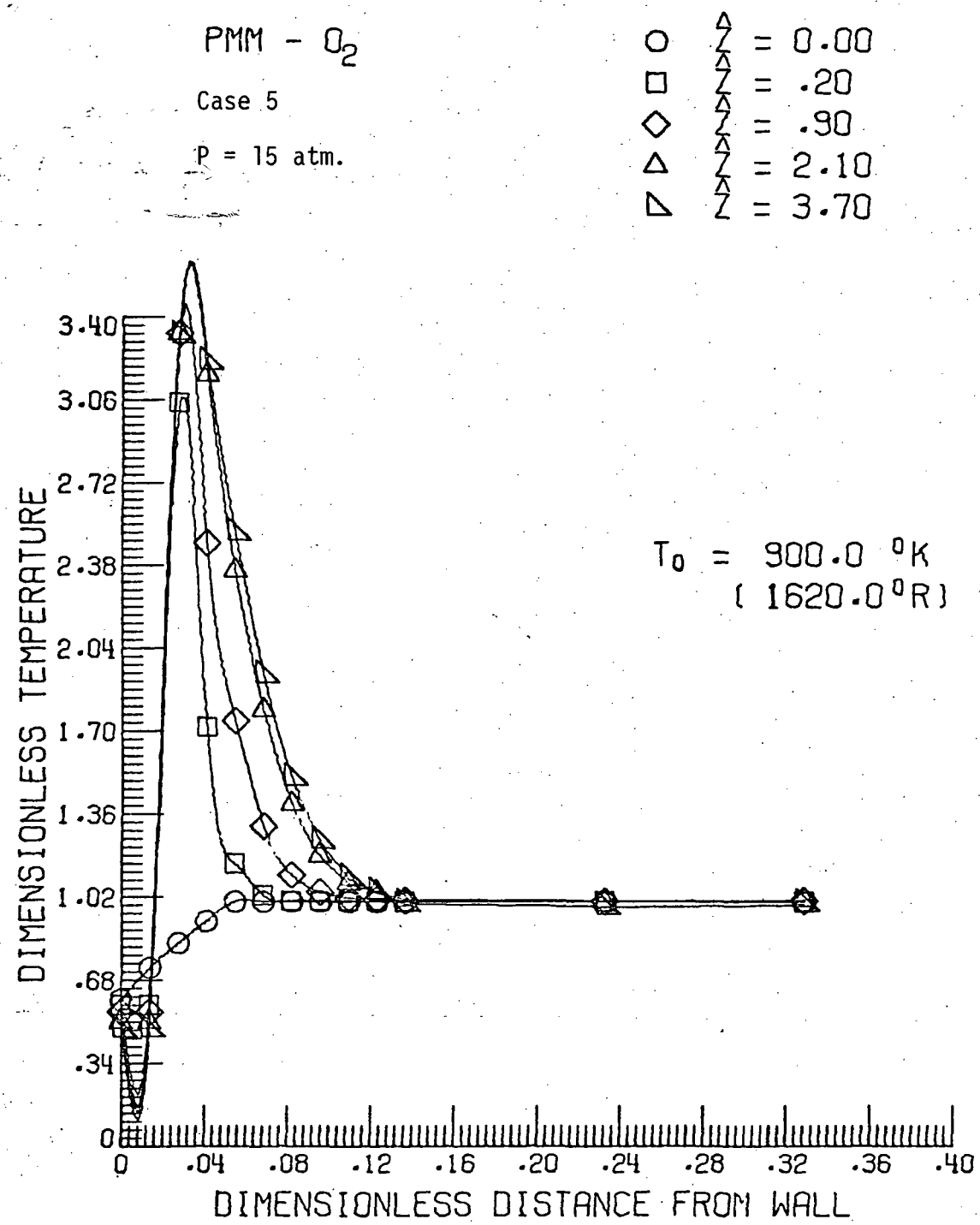

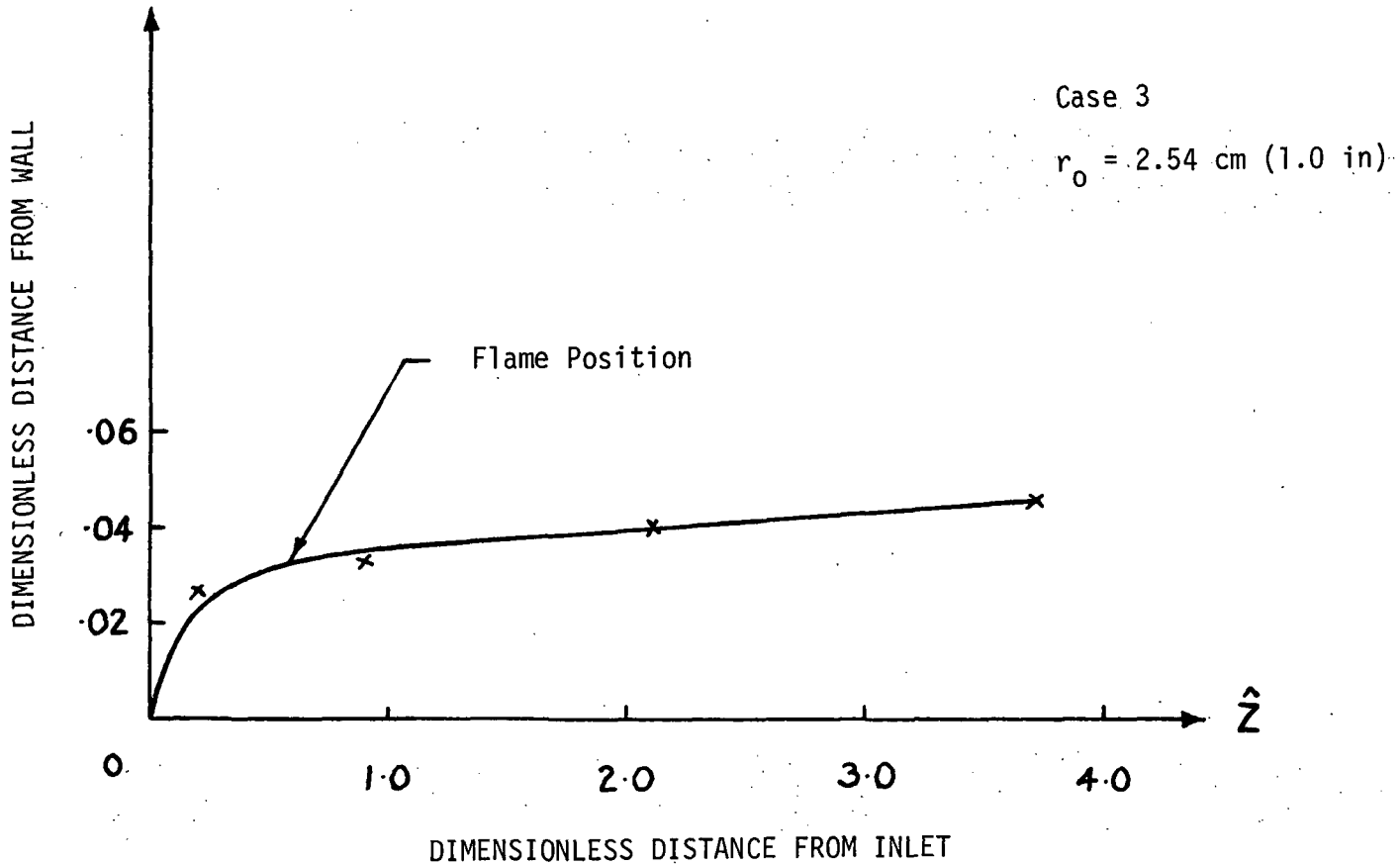

FIGURE 11. STEADY-STATE FLAME POSITION IN COMBUSTION CHAMBER

DISTRIBUTION LIST

Copy No.	
1 - 5	National Aeronautics and Space Administration Langley Research Center, Mail Stop 126 Hampton, Virginia 23365
- -	Contract NAS1-10210, Task Order #3
6 - 7	W.S.Y. Hung
8	C.S. Chen
9	J.K. Haviland
10	R.A. Lowry
11	J.J. Kauzlarich
12	C.B. Thomas
13 - 17	RLES Files

RESEARCH LABORATORIES FOR THE ENGINEERING SCIENCES

THORNTON HALL • UNIVERSITY OF VIRGINIA • CHARLOTTESVILLE 22901

November 17, 1972

NASA Scientific & Technical Information Facility
P. O. Box 33
College Park, Maryland 20740

Reference: NASA CR-112201

Gentlemen:

Enclosed are twelve (12) copies and one reproducible of our Final Report entitled "Further Analytical Study of Hybrid Rocket Combustion," by W. S. Y. Hung, C. S. Chen and J. K. Haviland of the Departments of Mechanical Engineering and Aerospace Engineering. Appropriate copies have been sent to the provided distribution list. Also, notification has been made to the Langley Contracting Officer.

If we may be of further assistance, please do not hesitate to contact us.

Sincerely,

R. A. Nixon

(Mrs.) R. A. Nixon
Publications Supervisor

RAN:mms

Enclosures (13): RLES Final Report No. AEEP-4041-106-72U

cc: Provided Distribution List
W. S. Y. Hung
C. S. Chen
J. K. Haviland
I. A. Fischer
B. F. Blaisdell
G. A. McAlpine
F. V. Moore
W. H. Grant